

Converting one photon into two via four-wave mixing in optical fibers

Audrey Dot,^{1,*} Evan Meyer-Scott,¹ Raja Ahmad,² Martin Rochette,² and Thomas Jennewein¹

¹*Institute for Quantum Computing and Department of Physics and Astronomy,
University of Waterloo, 200 University Ave W, Waterloo, Ontario, Canada, N2L 3G1*

²*Department of Electrical and Computer Engineering, McGill University,
3480 rue University, Montreal, Quebec, Canada, H3A 2A7*

Observing nonlinear optical quantum effects or implementing quantum information protocols using nonlinear optics requires moving to ever-smaller input light intensities. However, low light intensities generally mean weak optical nonlinearities, inadequate for many applications. Here we calculate the performance of four-wave mixing in various optical fibers for the case where one of the input beams is a single photon. We show that in tapered chalcogenide glass fibers (microwires) a single photon plus strong pump beam can produce a pair of photons with probability 0.1%, much higher than in previous work on bulk and waveguided crystal sources. Such a photon converter could be useful for creating large entangled photon states, for performing a loophole-free test of Bell's inequalities, and for quantum communication.

I. INTRODUCTION

Pairs of photons created via Spontaneous Parametric Down-Conversion (SPDC) [1] or spontaneous Four-Wave Mixing (FWM) [2] in a nonlinear optical material with a high-intensity pump laser have been used in many experiments in quantum optics, quantum metrology, and optical quantum information processing. Interest is increasingly converging on using SPDC or FWM in later stages of quantum information protocols, rather than just initial sources of photons [3–5]. This requires operation with very low intensity input states, including converting a single photon into a pair.

Should an efficient one-to-two photon conversion be realized, one important application is the entangling of three or more photons [6, 7]. These large entangled photon states are useful in quantum communication protocols [8, 9], and allow fundamental tests of quantum mechanics [7, 10, 11]. Increased efficiency in converting single photons to pairs would allow larger states to be generated, and with greater speed. Single photon conversion could also be used for heralding photons after long-distance transmission to close the Bell test detection loophole [12] and for device-independent quantum key distribution [13]; any improvement in conversion efficiency directly increases the communication rates. Finally, if efficient enough, single photon conversion could also be used directly in quantum computing as a two-qubit gate [14].

The key challenge in converting a single photon into a pair is the low efficiency of nonlinear optical processes at ultralow power. In principle, standard SPDC or FWM sources could be used, but the low efficiency (less than 10^{-5}) limits the single photon conversion to rates too low to be useful [15]. Therefore we consider here specialty fiber media, which we show can result in large conversion efficiencies thanks to long length, small core size, and

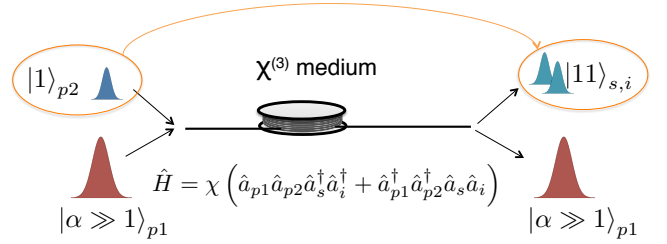


FIG. 1. [Color online] Four-wave mixing (FWM) with single photon and strong pump inputs. The toy Hamiltonian with interaction parameter χ illustrates the processes, but the full development is given in the text.

high nonlinearity.

We present complete calculations and simulations of FWM between a strong pump and a single photon as illustrated schematically in Fig. 1. First we set up the theoretical framework by extending the quantum theory of nondegenerate FWM [16, 17] to the single photon pump case. Then we apply the expressions to birefringent silica fibers, microstructured silica fibers, and chalcogenide microwires to find the spectra and conversion efficiency of the generated two-photon states.

II. QUANTUM THEORY OF FWM PUMPED BY A SINGLE PHOTON AND STRONG LASER

A. Equations of motion for a $\chi^{(3)}$ nonlinear medium

We determine the operator evolution of a system consisting of a strong pump beam and a single photon entering a nonlinear, dispersive, single mode fiber, and undergoing four-wave mixing and phase modulation as in Fig. 1. We proceed in the Heisenberg representation by solving the equation of motion for the field amplitude operators [18]. The two pumping fields are considered monochromatic or quasi-monochromatic, and we include

* audreyddot@gmail.com

self- and cross-phase modulation, but not parasitic effects such as Raman scattering and multi-photon absorption due to the low power of the inputs. We stay in the low gain regime, which means that only spontaneous FWM (also called Four Photon Scattering) is studied. This approximation stands if the total probability of generating a photon pair during the interaction is much lower than 1, and certainly holds since one of our pumps is a single photon.

The field is quantized in one dimension in a length large enough for the electric field to be written in the continuous limit [19]. We then choose for convenience to write this field in the frequency space, as a sum of its space-dependent spatial mode operators, an approach introduced in Ref. [18]. The quantization time T , equal to the quantization length divided by the speed of light, is then the time periodicity of the field, and the density of the frequency space is $\delta\omega = 2\pi/T$. T has to be long enough to allow the writing of the frequency modes in the continuous limit. The electric field is then

$$\begin{aligned} \hat{E}(r, t) = \sum_{j=x,y} \left(F(x, y) \sqrt{\frac{\hbar}{2\varepsilon_0 c}} \frac{1}{\sqrt{2\pi}} \right. \\ \left. \times \int d\omega \sqrt{\frac{\omega}{n_j(\omega)}} \hat{a}_j(\omega, z) e^{-i\omega t} + h.c. \right) \vec{e}_j, \end{aligned} \quad (1)$$

where the frequency integral runs from 0 to $+\infty$, and "h.c." stands for hermitian conjugate. $F(x, y)$, with $\iint |F(x, y)|^2 dx dy = 1$, is the transverse distribution of the fiber mode. The unit vectors \vec{e}_j describe the field's polarization, and $n_j(\omega)$ is the effective index of refraction for the fiber mode of frequency ω and polarization j . Since in the continuous limit, we approximated the discrete longitudinal modes of a laser cavity by continuous mode annihilation operators, $\hat{a}_j(\omega, z)$, with units of inverse square root frequency [19]. They follow the commutation relations $[\hat{a}_j(\omega, z), \hat{a}_{j'}^\dagger(\omega', z)] = \delta(\omega - \omega') \delta_{jj'}$, with Dirac delta $\delta(\omega - \omega')$ and Kroenecker delta $\delta_{jj'}$.

These operators $\hat{a}_j(\omega, z)$ and the quantum state of the system $|\psi\rangle$ provide complete knowledge about the state as a function of propagation distance z , which allows us to extract the efficiency of single photon to pair conversion. In the Heisenberg representation, $|\psi\rangle$ is constant and we only need to solve for the evolution of the annihilation operators.

If considering only one polarization component, the propagating field can be simplified into

$$\begin{aligned} \hat{E}(z, t) = \sqrt{\frac{\hbar}{4\pi\varepsilon_0 c A_{\text{eff}}}} \int d\omega \sqrt{\frac{\omega}{n(\omega)}} \hat{a}(\omega, z) e^{-i\omega t} + h.c. \\ = \hat{E}^{(+)}(z, t) + \hat{E}^{(-)}(z, t), \end{aligned} \quad (2)$$

where the transverse modal distribution was also simplified using the effective area of the fiber mode $A_{\text{eff}} = \frac{1}{\iint |F(x, y)|^4 dx dy}$, taken to be the same for all the frequency components in the fiber.

The evolution equation of the annihilation operators can be given by

$$\frac{\partial \hat{a}(\omega, z)}{\partial z} = \frac{i}{\hbar} [\hat{a}(\omega, z), \hat{G}(z)], \quad (3)$$

where the momentum operator \hat{G} is given by integration over the cross-sectional area of the momentum that flows during the quantization time.

$$\hat{G}(z) = \int_{A_{\text{eff}}} dS \int_0^T dt \hat{D}^{(-)}(z, t) \hat{E}^{(+)}(z, t) + h.c., \quad (4)$$

where $\hat{D}(z, t) = \varepsilon_0 \hat{E}(z, t) + \hat{P}(z, t)$ is the electric displacement operator. The polarization operator is defined by

$$\begin{aligned} \hat{P}(z, t) = \sum_{n \geq 1} \varepsilon_0 \chi^{(n)} \cdot \hat{E}^n(z, t) \\ = \hat{P}_l(z, t) + \hat{P}_{nl}(z, t), \end{aligned} \quad (5)$$

which is the sum of the linear polarization $\hat{P}_l(z, t)$ given by $\varepsilon_0 \chi^{(1)}(\omega) \cdot \hat{E}(r, t)$, and the nonlinear polarization $\hat{P}_{nl}(z, t)$ of higher orders. We can thus separate $\hat{G}(z)$ into linear and nonlinear parts as $\hat{G}(z) = \hat{G}_l(z) + \hat{G}_{nl}(z)$, driven by corresponding linear and nonlinear polarizations.

The linear evolution of the momentum operator is obtained from Eqs. (2), (4), and (5) as (see Appendix A)

$$\hat{G}_l(z) = \int d\omega \hbar \beta(\omega) \hat{a}^\dagger(\omega, z) \hat{a}(\omega, z), \quad (6)$$

with the propagation constant $\beta(\omega) = \frac{n(\omega)\omega}{c}$. The linear evolution of any annihilation operator can thus be deduced from Eqs. (3) and (6) as

$$\hat{a}_l(\omega, z) = \hat{a}_0(\omega, z) e^{i\beta(\omega)z}. \quad (7)$$

The nonlinear evolution (contained in $\hat{a}_0(\omega, z)$) can be found similarly from the nonlinear evolution of the momentum. \hat{G}_{nl} can be decomposed into two parts as $\hat{G}_{nl}(z) = \hat{G}_{nl}^{FWM}(z) + \hat{G}_{nl}^{ph\ mod}(z)$ (see Appendix A), one giving FWM and the other phase modulation.

The two pumping fields, of frequencies $\omega_{p1,2}$, are considered monochromatic or quasi-monochromatic, perfectly overlapping in time, and have the same spectral bandwidth $\delta\omega_p$ with $\delta\omega_p/\omega_{p1,2} \ll 1$. It is convenient to choose the quantization time as the Fourier transform of the pulses' spectral width, $T = 2\pi/\delta\omega_p$. The frequency-space density is therefore $\delta\omega = \delta\omega_p$. For monochromatic pumps, this quantization time, as well as the pulse duration, is infinite.

The FWM part of the momentum operator is (see Appendix A)

$$\hat{G}_{nl}^{FWM}(z) = 3\chi^{(3)} \frac{\hbar^2}{\varepsilon_0 c^2 A_{\text{eff}} T} \times \frac{2\pi}{T} \left[\int d\omega \sqrt{\frac{\omega \omega_{p1} \omega_{p2} (\omega_{p1} + \omega_{p2} - \omega)}{n(\omega) n(\omega_{p1}) n(\omega_{p2}) n(\omega_{p1} + \omega_{p2} - \omega)}} \hat{a}_0^\dagger(\omega, z) \hat{a}_0^\dagger(\omega_{p1} + \omega_{p2} - \omega, z) \hat{a}_0(\omega_{p1}, z) \hat{a}_0(\omega_{p2}, z) e^{-i\Delta k z} + h.c. \right] \quad (8)$$

with $\Delta k = \beta(\omega) + \beta(\omega_{p1} - \omega_{p2} - \omega) - \beta(\omega_{p1}) - \beta(\omega_{p2})$, and where the integral over ω covers the whole positive spectrum except the two injected frequencies. The two creation operators $\hat{a}_0^\dagger(\omega, z) \hat{a}_0^\dagger(\omega_{p1} + \omega_{p2} - \omega, z)$ indicate that output photons can only be created in pairs, with correlated frequencies ω and $\omega_{p1} + \omega_{p2} - \omega$.

The phase modulation part is (see Appendix A)

$$\begin{aligned} \hat{G}_{nl}^{ph\,mod}(z) = 3\chi^{(3)} \frac{\hbar^2}{\varepsilon_0 c^2 A_{\text{eff}} T} & \left[\iint d\omega d\omega' \frac{\omega}{n(\omega)} \frac{\omega'}{n(\omega')} \right. \\ & \times \hat{a}_0^\dagger(\omega, z) \hat{a}_0(\omega', z) \hat{a}_0^\dagger(\omega', z) \hat{a}_0(\omega, z) \\ & \left. - \frac{1}{2} \int d\omega \times \frac{2\pi}{T} \left(\frac{\omega}{n(\omega)} \hat{a}_0^\dagger(\omega, z) \hat{a}_0(\omega, z) \right)^2 \right], \end{aligned} \quad (9)$$

with the integrals covering the whole positive spectrum.

We can now derive the evolution of the mode operators from Eq. (3), for any frequency generated in the fiber.

$$\begin{aligned} \frac{\partial \hat{a}_0(\omega, z)}{\partial z} = 3i\chi^{(3)} \frac{\hbar}{\varepsilon_0 c^2 A_{\text{eff}} T} \times & \left[\frac{2\pi}{T} \sqrt{\frac{\omega \omega_{p1} \omega_{p2} (\omega_{p1} + \omega_{p2} - \omega)}{n(\omega) n(\omega_{p1}) n(\omega_{p2}) n(\omega_{p1} + \omega_{p2} - \omega)}} \right. \\ & \times \hat{a}_0^\dagger(\omega_{p1} + \omega_{p2} - \omega, z) \hat{a}_0(\omega_{p1}, z) \hat{a}_0(\omega_{p2}, z) e^{-i\Delta k z} \\ & + \frac{\omega}{n(\omega)} \int d\omega' \frac{\omega'}{n(\omega')} \left[\hat{a}_0^\dagger(\omega', z) \hat{a}_0(\omega', z) + \frac{1}{2} \frac{T}{2\pi} \right] \hat{a}_0(\omega, z) \\ & \left. - \frac{1}{2} \frac{2\pi}{T} \frac{\omega^2}{n(\omega)^2} \hat{a}_0^\dagger(\omega, z) \hat{a}_0(\omega, z) \hat{a}_0(\omega, z) \right]. \end{aligned} \quad (10)$$

The first of the two summed terms reflects the evolution by FWM and the second the self-phase modulation. If we neglect the phase modulation arising from the generated frequencies as these will be much weaker than the pumps, we have, for the generated frequencies,

$$\begin{aligned} \frac{\partial \hat{a}_0(\omega, z)}{\partial z} = 3i\chi^{(3)} \frac{\hbar}{\varepsilon_0 c^2 A_{\text{eff}} T} \times \frac{2\pi}{T} & \left[\sqrt{\frac{\omega \omega_{p1} \omega_{p2} (\omega_{p1} + \omega_{p2} - \omega)}{n(\omega) n(\omega_{p1}) n(\omega_{p2}) n(\omega_{p1} + \omega_{p2} - \omega)}} \hat{a}_0^\dagger(\omega_{p1} + \omega_{p2} - \omega, z) \hat{a}_0(\omega_{p1}, z) \hat{a}_0(\omega_{p2}, z) e^{-i\Delta k z} + \right. \\ & \left. \frac{\omega}{n(\omega)} \left[\frac{\omega_{p1}}{n(\omega_{p1})} \hat{a}_0^\dagger(\omega_{p1}, z) \hat{a}_0(\omega_{p1}, z) + \frac{\omega_{p2}}{n(\omega_{p2})} \hat{a}_0^\dagger(\omega_{p2}, z) \hat{a}_0(\omega_{p2}, z) + \frac{1}{2} \frac{\omega}{n(\omega)} \frac{T}{2\pi} \right] \hat{a}_0(\omega, z) \right]. \end{aligned} \quad (11)$$

For the incoming pump frequencies the evolution is given by

$$\begin{aligned} \frac{\partial \hat{a}_0(\omega_j, z)}{\partial z} = 3i\chi^{(3)} \frac{\hbar}{\varepsilon_0 c^2 A_{\text{eff}} T} \times & \left[\int d\omega \sqrt{\frac{\omega \omega_j \omega_k (\omega_j + \omega_k - \omega)}{n(\omega) n(\omega_j) n(\omega_k) n(\omega_j + \omega_k - \omega)}} \hat{a}_0(\omega, z) \hat{a}_0(\omega_{p1} + \omega_{p2} - \omega, z) \hat{a}_0^\dagger(\omega_k, z) e^{i\Delta k z} + \right. \\ & \left. \frac{2\pi}{T} \frac{\omega_j}{n(\omega_j)} \left[\frac{1}{2} \frac{\omega_j}{n(\omega_j)} \hat{a}_0^\dagger(\omega_j, z) \hat{a}_0(\omega_j, z) + \frac{\omega_k}{n(\omega_k)} \hat{a}_0^\dagger(\omega_k, z) \hat{a}_0(\omega_k, z) + \frac{1}{2} \frac{\omega}{n(\omega)} \frac{T}{2\pi} \right] \hat{a}_0(\omega_j, z) \right], \end{aligned} \quad (12)$$

with $j, k = p1, p2$,

Though we are in the quasi-monochromatic approximation, the pumps' creation and annihilation operators are not dimensionless, for homogeneity with those of the generated modes.

B. Solution for a single photon and a strong pump

To solve Eqs. (11) and (12), the strong pump is taken as classical ($\hat{a}_0(\omega_{p1}, z) \equiv A_{p1}(z)$), and undepleted ($|A_{p1}(z)|^2 = |A_{p1}(0)|^2$). The weak pump, $p2$, has to be kept quantum throughout, since it is on the few- or single-photon level. Therefore we can also assume the number of

weak pump photons is negligible compared to the number of strong pump photons and so neglect phase modulation from the weak pump.

We use the standard waveguide nonlinear parameter $\gamma(\omega) = \frac{3\chi^{(3)}\omega}{2\varepsilon_0 c^2 n(\omega)^2 A_{\text{eff}}}$. If all the frequencies are close, we can use the same, averaged γ for all the frequency modes, which is commonly used to simplify the notation but is not necessary for the solution [20].

With these approximations the evolution of the strong pump can be simplified from Eq. (12) to

$$\frac{dA_{p1}(z)}{dz} = i\gamma P_1 A_{p1}(z), \quad (13)$$

where we defined the pump peak power as $P_1(z) = \frac{\hbar\omega_{p1} \times N_1(z)}{T} = \frac{2\pi\hbar\omega_{p1}}{T^2} \times |A_{p1}(z)|^2$. Here $N_1(z) = \frac{2\pi}{T} |A_{p1}(z)|^2$ is the number of pump photons going through a plane at position z per time T . In the undepleted pump approximation, P_1 is independent of z .

Equation (13) is solved as [21]

$$A_{p1}(z) = A_{p1}(0)e^{i\gamma P_1 z}. \quad (14)$$

The evolution of the weak pump can then be simplified from Eq. (12) to

$$\frac{\partial \hat{a}_0(\omega_{p2}, z)}{\partial z} = \frac{2i\gamma\hbar}{T} \int d\omega \sqrt{\omega(\omega_{p1} + \omega_{p2} - \omega)} A_{p1}^*(0) e^{-i\gamma P_1 z} \hat{a}_0(\omega, z) \hat{a}_0(\omega_{p1} + \omega_{p2} - \omega, z) e^{i\Delta k z} + 2i\gamma P_1 \hat{a}_0(\omega_{p2}, z), \quad (15)$$

and if we choose $A_{p1}^*(0) = A_{p1}(0) = T\sqrt{\frac{P_1}{2\pi\hbar\omega_{p1}}}$ then

$$\frac{\partial \hat{a}_0(\omega_{p2}, z)}{\partial z} = 2i\gamma \left[\sqrt{P_1} \sqrt{\frac{\hbar}{2\pi\omega_{p1}}} \int d\omega \sqrt{\omega(\omega_{p1} + \omega_{p2} - \omega)} \hat{a}_0(\omega, z) \hat{a}_0(\omega_{p1} + \omega_{p2} - \omega, z) e^{i(\Delta k - \gamma P_1)z} + P_1 \hat{a}_0(\omega_{p2}, z) \right]. \quad (16)$$

We can write this more explicitly by introducing $\zeta_2 = \frac{2\pi\hbar\omega_{p2}}{T^2}$, where $\zeta_2 \times \langle \hat{a}^\dagger(\omega_{p2}, 0) \hat{a}(\omega_{p2}, 0) \rangle = P_2$ is the peak power of the weak pump at the medium entrance, with $P_2 = \zeta_2 \times \frac{T}{2\pi}$ in case of a single photon pumping. We then have

$$\frac{\partial \hat{a}_0(\omega_{p2}, z)}{\partial z} = 2i\gamma \left[\sqrt{P_1} \sqrt{\zeta_2} \frac{2\pi}{T} \int d\omega \hat{a}_0(\omega, z) \hat{a}_0(\omega_{p1} + \omega_{p2} - \omega, z) e^{i(\Delta k - \gamma P_1)z} + P_1 \hat{a}_0(\omega_{p2}, z) \right]. \quad (17)$$

Finally, the evolution of the generated modes' annihilation operators, simplified from Eq. (11), is

$$\frac{\partial \hat{a}_0(\omega, z)}{\partial z} = 2i\gamma \left[\sqrt{\zeta_2} \sqrt{P_1} \hat{a}_0^\dagger(\omega_{p1} + \omega_{p2} - \omega, z) \hat{a}_0(\omega_{p2}, z) e^{-i(\Delta k - \gamma P_1)z} + P_1 \hat{a}_0(\omega, z) \right]. \quad (18)$$

The evolution of both the weak pump and of the generated photons can be derived in the low gain approximation by using a Baker-Hausdorff expansion to first order in the effective gain $\gamma\sqrt{T\zeta_2}\sqrt{P_1}L \ll 1$. The calculations for the annihilation operators of the generated frequencies are detailed in Appendix B and give the main result

$$\hat{a}_0(\omega, L) e^{-i2\gamma P_1 L} = \hat{a}_0(\omega, 0) + 2i\gamma \times \sqrt{P_1} \sqrt{\zeta_2} L e^{-i\frac{KL}{2}} \text{sinc}\left(\frac{KL}{2}\right) \times \hat{a}_0^\dagger(\omega_{p1} + \omega_{p2} - \omega, 0) \hat{a}_0(\omega_{p2}, 0), \quad (19)$$

where $K = \Delta k + \gamma P_1 = \beta(\omega) + \beta(\omega_{p1} + \omega_{p2} - \omega) - \beta(\omega_{p1}) - \beta(\omega_{p2}) + \gamma P_1$ is the total phase mismatch, sum of the linear and nonlinear parts.

Note that by considering only the first order gain, we assume that the conversion efficiency is low enough to be well represented by a single conversion process, described by $\hat{a}_0(\omega_{p1}, L) \hat{a}_0(\omega_{p2}, L) \hat{a}_0^\dagger(\omega, L) \hat{a}_0^\dagger(\omega_{p1} + \omega_{p2} - \omega, L)$. We neglect the reverse process of converting the pairs back to pump photons, which is equivalent to neglecting double-pair emissions in SPDC or standard FWM. This approximation causes deviation less than 2×10^{-6} for conversion efficiency $\eta = 0.1\%$, and less than 0.02 for a single photon conversion efficiency up to $\eta = 10\%$, as discussed in Appendix C. A treatment without the low gain approximation would allow simulation of Rabi oscillations

between the single photon and photon pair, as required for the coherent photon conversion of Ref. [14].

III. SINGLE PHOTON CONVERSION EFFICIENCY

The conversion efficiency of the single photon into a pair can now be derived from Eq. (19). The spectral density of the photons created during the characteristic

time T is given by

$$n_d(\omega, L) = \left\langle \psi \left| \hat{a}_0^\dagger(\omega, L) \hat{a}_0(\omega, L) \right| \psi \right\rangle. \quad (20)$$

The quantum state $|\psi\rangle$ is the input state of the weak pump and generated photon pairs. For a single photon on pump 2, $|\psi\rangle = |1\rangle_{p2} |0\rangle_s |0\rangle_i$, where we label the lower frequency half of the output pair spectrum *idler*, and the higher half *signal*. The total number of photons generated during T is then given by the integral of the spectral density over the output spectrum.

Putting Eq. (19) into Eq. (20) gives the photon number spectral density per characteristic time

$$\begin{aligned} n_d(\omega, L) &= \frac{T}{2\pi} \times 4\gamma^2 P_1 P_2 L^2 \text{sinc}^2 \left(\frac{KL}{2} \right) \\ &= 4\gamma^2 P_1 \frac{\hbar\omega_{p2}}{2\pi} L^2 \text{sinc}^2 \left(\frac{KL}{2} \right), \end{aligned} \quad (21)$$

where the generation of a photon at frequency ω implies the generation of its pair photon at frequency $\omega_{p1} + \omega_{p2} - \omega$. Let us now find the total number of photon pairs generated out of a single photon in cases of pulsed and continuous-wave pumping.

A. Regime with both pumps pulsed

If both pumps are pulsed simultaneously with a spectral width $\delta\omega_p$ and $T = \frac{2\pi}{\delta\omega_p}$, the total number of photon pairs generated per time T (or per pulse for transform-limited pulses) is

$$\begin{aligned} N_{\text{pairs/pulse}} &= \frac{1}{2} \int d\omega n_d(\omega, L) \\ &= 4\gamma^2 P_1 P_2 L^2 \frac{\Delta\omega_s}{\delta\omega_p} \\ &= 4\gamma^2 P_1 \frac{\hbar\omega_{p2}}{2\pi} L^2 \Delta\omega_s, \end{aligned} \quad (22)$$

with

$$\Delta\omega_s = \frac{1}{2} \int d\omega \text{sinc}^2 \left(\frac{K(\omega_{p1}, \omega_{p2}, \omega)L}{2} \right) \quad (23)$$

and $P_2 = \frac{\hbar\omega_{p2}}{T}$, where the factor 1/2 in the first line is due to the spectrum covering both signal and idler frequencies, leading to double-counting. The integral is over the whole spectral range except the two pump frequencies $\omega_{p1, p2}$.

The number of generated photons pairs per second is thus

$$\begin{aligned} N_{\text{pairs/sec}} &= f_{\text{rep}} \times 4\gamma^2 P_1 P_2 L^2 \frac{\Delta\omega_s}{\delta\omega_p} \\ &= 4\gamma^2 P_{1\text{avg}} P_2 L^2 \frac{\Delta\omega_s}{2\pi}, \end{aligned} \quad (24)$$

with $P_1 = \frac{P_{1\text{avg}}}{f_{\text{rep}}} \times \frac{\delta\omega_p}{2\pi}$, where f_{rep} is the repetition rate of the source.

B. Regime with one pump pulsed and the other continuous-wave

If one of the pumps is pulsed and the other is continuous-wave (CW), the output photons will behave as if both pumps were pulsed at the repetition rate of the pulsed one, which removes the necessity for time alignment. Taking the single photon pump as pulsed and the strong pump as CW, we have $P_1 = P_{1\text{avg}}$ and $P_2 = \frac{\hbar\omega_{p2}}{T}$, which gives

$$N_{\text{pairs/sec}} = f_{\text{rep}} \times 4\gamma^2 P_{1\text{avg}} P_2 L^2 \frac{\Delta\omega_s}{\delta\omega_p}. \quad (25)$$

The pair generation is independent of the single photon pulse duration, depending only on its repetition rate and the strong laser's CW pump power. It is less efficient by a factor $\frac{f_{\text{rep}}}{\delta\omega_p}$ compared to when both pumps are pulsed.

If we want the weak pump to be CW, we can argue an “equivalent single photon” pumping such that each pulse of the strong pump sees on average one photon of the weak pump. Then we have to take $P_2 = P_{2\text{avg}} = \frac{\hbar\omega_{p2}}{T}$, and

$$N_{\text{pairs/sec}} = 4\gamma^2 P_{1\text{avg}} P_{2\text{avg}} L^2 \frac{\Delta\omega_s}{2\pi}. \quad (26)$$

This generation is equivalent to the pulsed/pulsed pumping, which is not surprising since the “equivalent single photon” pumping is CW pumping with the same peak power as the pulsed pumping. This means many more photons of pump p2 enter the fiber, but only the ones which overlap a strong pump pulse can convert into pairs.

C. Regime with two continuous-wave pumps

With an input made out of a weak continuous pump 2 and a strong continuous pump 1, then the number of photons generated per second is straightforward,

$$N_{\text{pairs/sec}} = 4\gamma^2 P_{1\text{avg}} P_{2\text{avg}} L^2 \frac{\Delta\omega_s}{2\pi}, \quad (27)$$

however it is not obvious to define what qualifies as a single photon for a CW pump. This regime can reach the same efficiency as the pulsed/pulsed case if either of the pumps' CW average power is raised to the peak power of the pulsed/pulsed case. This would be difficult in practice, as peak powers can be four orders of magnitude larger than average powers for the example of modelocked picosecond lasers.

IV. CANDIDATE FIBERS FOR MAXIMIZING CONVERSION EFFICIENCY

In this section we compare three fiber types with unique methods of phasematching to find the best for single photon conversion. The single photon conversion efficiency can be defined, for a weak pumping field composed of N_{p2} photons per time unit, as $\eta = \frac{N_{\text{pairs}}}{N_{p2}}$, N_{pairs} being the number of photon pairs generated during the same time unit. If the weak pumping field is a single photon, the pulsed/pulsed configuration gives the highest conversion efficiency for a given input average power of pump 1 (compare Eq. (24) with Eqs. (25) and (27)). Let us consider strategies for maximizing the single photon conversion in this regime. When $N_{p2} = 1$, the conversion efficiency as given by Eq. (22) is

$$\eta = \frac{N_{\text{pairs}}}{N_{p2}} = 4\gamma^2 P_1 \frac{\hbar\omega_{p2}}{2\pi} L^2 \Delta\omega_s. \quad (28)$$

The parameters that can be tuned to maximize conversion efficiency are nonlinearity $\chi^{(3)}$ and mode area A_{eff} through γ , length L , phasematching bandwidth $\Delta\omega_s$, and peak power P_1 of the strong pump. Since γ is squared, decreasing A_{eff} and increasing $\chi^{(3)}$ will have the greatest effect. By contrast, conversion efficiency appears quadratic in the length of fiber, L , but the signal and idler bandwidths given by Eq. (23) will vary approximately with $1/L$, giving an overall linear dependence on fiber length. The spectral width $\Delta\omega_s$ can also vary independent of L from tiny ($\delta\omega$) to hundreds of nano-meters, depending on the pump configuration, and most importantly on the type of phasematching chosen.

We examine three candidates for maximizing conversion efficiency, corresponding to the three main methods of phasematching in optical fibers: birefringence, operation near a zero dispersion wavelength (ZDW), and nonlinear phasematching using self-phase modulation. The phasematched frequencies generated by the use of birefringence are spectrally narrow and highly tunable. The frequencies phasematched around the ZDW or due to nonlinear phase modulation can have a broader spectrum, and are centered around or near the ZDW. We compare the potential for single photon conversion in three different fiber types corresponding to those three types of phasematching, and find the optimal parameters to maximize pair generation.

The phase mismatch can be expressed as a Taylor expansion around the central frequency ω_0 as

$$K(\Omega) = \beta_2(\omega_0) (\Omega^2 - \Delta\omega^2) + \frac{\beta_4(\omega_0)}{12} (\Omega^4 - \Delta\omega^4) + \gamma P_1, \quad (29)$$

with the central frequency $\omega_0 = \frac{\omega_{p2} + \omega_{p1}}{2}$, the offset frequency $\Omega = \omega - \omega_0$, the pump offset $\Delta\omega = \frac{\omega_{p2} - \omega_{p1}}{2}$, and dispersion coefficients given by

$$\beta_i(\omega_0) = \left(\frac{\partial^i \beta(\omega)}{\partial \omega^i} \right)_{\omega_0}. \quad (30)$$

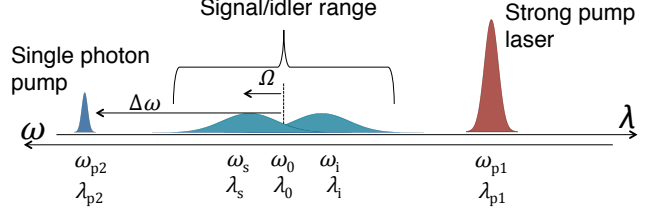


FIG. 2. [Color online] Arrangement of pump and signal/idler wavelengths (amplitudes and widths not to scale). The main source of noise, spontaneous Raman scattering from the strong pump, will occur to the far right of this figure, allowing its removal by spectral filtering.

Two schemes can be considered when the pump wavelengths are nondegenerate as required for single-photon FWM: external pumping, with generation of new wavelengths in between the pump wavelengths, or internal pumping, with generation of new wavelengths to the exterior. We focus on external pumping as illustrated in Fig. 2 because, assuming the strong pump has the highest wavelength, it allows filtering the main Raman noise from the strong pump as this will be at higher wavelengths still. However, the large separation in pump wavelengths can lead to temporal walk-off between the pump pulses in the fiber, reducing efficiency. This effect is mitigated by situating the pumps symmetrically about the ZDW.

A. Polarization maintaining fiber: birefringent phasematching

Standard polarization maintaining (PM) fiber exhibits a birefringence large enough to achieve phasematching some dozens to hundreds of tera-hertz from the pumps (~ 100 nm) [22]. These fibers are commercially available, with lengths up to kilometers, and spatially uniform. The phasematching is easy to obtain and widely tunable by tuning the pump wavelengths. Further, the birefringent phasematching means that the photon pairs can come out with opposite polarizations from the pumps, enabling polarization filtering of the pumps and associated Raman noise. However, the relatively large core size leads to a modest waveguide nonlinear parameter of $\gamma = 4.6 \times 10^{-3} \text{ W}^{-1} \cdot \text{m}^{-1}$ in our example below.

We consider the two pumps co-polarized along the fast axis and the generated signal and idler polarized along the slow axis, which gives total phase mismatch

$$K(\Omega) = \beta_2(\omega_0) (\Omega^2 - \Delta\omega^2) + \frac{\beta_4(\omega_0)}{12} (\Omega^4 - \Delta\omega^4) + \gamma P_1 + 2\omega_0 \frac{\delta n}{c}, \quad (31)$$

where the birefringence $\delta n = n^{\text{slow}} - n^{\text{fast}}$ is written separately from the dispersion coefficients. Far from the

ZDW ($\beta_2 \gg \beta_4, \gamma P_1$), the phase matched frequencies are

$$\Omega^2 = -\frac{2\omega_0}{\beta_2(\omega_0)} \frac{\delta n}{c} + \Delta\omega^2. \quad (32)$$

We consider a silica PM fiber with birefringence $\delta n = 3 \times 10^{-4}$ (e.g. Panda PM630), and take both pumps pulsed with 80 MHz repetition rate and 5 ps pulses. We take a 5 W average power for the strong pump, and a single photon for the weak pump. The walk-off length between the two pump pulses in this configuration being 18 cm, we consider an 11 cm fiber which gives an effective interaction length of $L = 10$ cm.

With the strong pump at 890 nm and the weak pump at 660 nm, we obtain a signal and idler phase matched at 728 nm and 790 nm with spectral width $\Delta\omega_s = 7$ rad THz (2 nm), as shown in Fig. 3. The conversion efficiency given by Eq. (28) is $\eta = 2 \times 10^{-8}$, well below that achievable in $\chi^{(2)}$ media. We plot the signal and idler spectral density (photons per (rad Hz) per pulse) in Fig. 3, accurate to the precision of our frequency space mapping, $\delta\omega_p = 1.3$ rad THz (0.5 nm, given by the width of the grey lines on the graph).

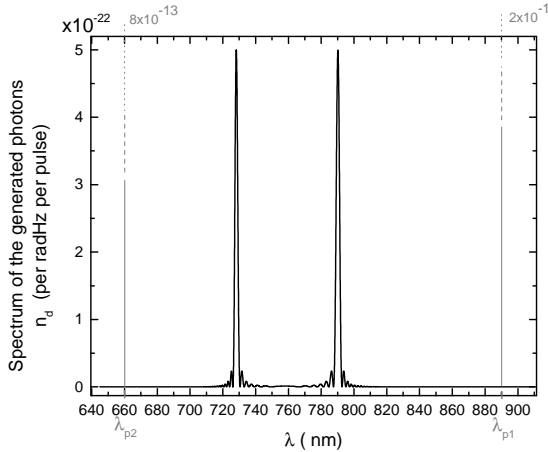


FIG. 3. Converting a single photon to a pair via FWM is possible in principle using a PM fiber, but the very narrow phasematching limits the efficiency to $\eta = 2 \times 10^{-8}$ in this example. The quasi-monochromatic pump wavelengths are represented by grey lines of width 1.3 rad THz with values labeled above the graph (well above the y-axis shown), while the generated signal and idler spectra are the black lines in the centre.

B. Microstructured fiber: phasematching near the zero-dispersion wavelength

Phasematching occurs in a fiber near the ZDW when the material and waveguide contributions to dispersion cancel. We will take the example of silica microstructured fibers, which are commercially available and can

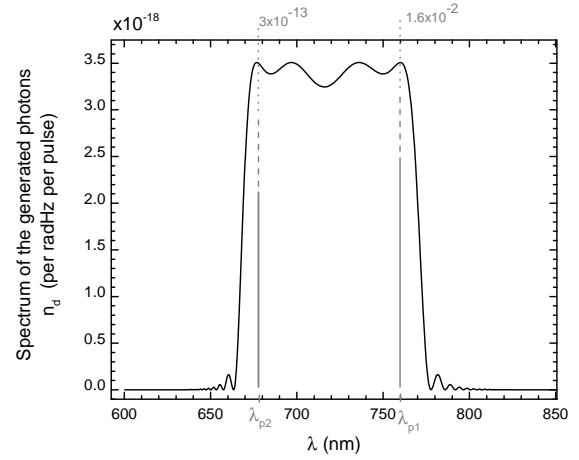


FIG. 4. A much broader signal and idler spectrum is obtained near the ZDW using a microstructured fiber. Even after filtering between 675 nm and 760 nm to remove noise photons near the pumps, the efficiency $\eta = 4 \times 10^{-4}$ over the remaining signal/idler range is four orders of magnitude larger than for the PM fiber. The grey lines represent the pumps' wavelengths, widths (now 3.1 rad THz) and intensity as in Fig. 3.

be fabricated to exhibit a ZDW in the visible and telecom ranges. The interest in such a fiber is that the core can be much smaller than regular single mode fibers, thus increasing the waveguide nonlinear parameter, e.g. up to $\gamma = 2.7 \times 10^{-2} \text{ W}^{-1} \cdot \text{m}^{-1}$ in our example, with lengths up to a few meters [23]. The spectral broadness of the phasematching depends on the length considered, and is only tuneable in a small range once the ZDW is chosen.

We model a microstructured fiber with core diameter of $1.8 \mu\text{m}$ and air fraction 0.72 in the cladding, which give the ZDW at 716 nm. The wavelengths and the pump powers are altered slightly from the previous example to achieve phasematching. We take a 1 W average power for the strong pump in a 2 m long fiber, with 2 ps long pump pulses and 2 ps long single photon pulses at 80 MHz repetition rate. As a consequence of working near the ZDW, the walkoff length is now over 100 m, since the pumps have approximately the same propagation constant β on either side of the ZDW. The single photon frequency is at wavelength 676.75 nm and the strong pump is now at 760 nm. Simulations give a much broader spectrum for the signal and idler (around 160 rad THz, Fig. 4), and consequently the efficiency, still given by Eq. (28), is now up to $\eta = 4 \times 10^{-4}$. Even including filtration of the generated photons between 686 nm and 750 nm to allow pump removal, this efficiency four orders of magnitude better than the PM fiber.

However, this method of phasematching is very sensitive to core diameter and pump wavelengths. For example, a 0.5 nm deviation of pump wavelength changes the output spectral shape completely and, even if still phase-

matched, may give no pairs at the center of the spectrum. Additionally, obtaining a 2 m microstructured fiber with good uniformity for the whole length is not straightforward, as some variations in the core diameter will occur that deteriorate the perfect phasematching.

C. Chalcogenide microwire fiber: phasematching due to self-phase modulation

Achieving the best conversion efficiency requires ultrahigh nonlinearity and small cross-sectional area. These can be achieved by tapering fibers made of chalcogenide glass as in Refs. [24, 25]. The chalcogenide As_2Se_3 has $\chi^{(3)}$ three orders of magnitude larger than that of silica glass and core diameters in the tapered microwire region can be as small as 500 nm thanks to its large refractive index, while still maintaining good coupling to standard single mode fiber and lengths beyond 10 cm. These microwires exhibit ultrahigh waveguide nonlinear parameters up to $\gamma = 180 \text{ W}^{-1}\cdot\text{m}^{-1}$.

This large γ directly leads to high conversion efficiency, but also allows nonlinear phasematching. As seen in Eq. (29) it is possible to compensate for positive or negative linear phase mismatch by the nonlinear contribution γP_1 due to the strong pump self-phase modulation. The higher the dispersive mismatch, the higher the pump powers must be to compensate, so moderate pump powers still require working near the ZDW. In the external pumping configuration of Fig. 2, the dispersion β_2 or β_4 has to be positive to compensate for self-phase modulation because the pump offset is greater than the frequency offset, i.e. $\Delta\omega^2 > \Omega^2$. The pump power necessary to reach perfect phasematching is

$$P_1 = \frac{1}{\gamma} \left(\beta_2(\omega_0)\Delta\omega^2 + \frac{\beta_4(\omega_0)}{12}\Delta\omega^4 \right). \quad (33)$$

For convenient all-telecom operation and to avoid the two-photon absorption at short wavelengths in chalcogenide glass As_2Se_3 [26], we take the example of the FWM scheme pumped at 1480 nm by the single photon and at 1620 nm by a strong pump. The two fields are pulsed at 80 MHz with 2 ps long pulses. The fiber considered is similar to the samples described in Ref. [25]. A fiber diameter of $0.555 \mu\text{m}$ for the microwire gives a dispersion coefficient at 1550 nm of $\beta_2(\omega_0) = 0.05 \text{ ps}^2/\text{m}$, and β_4 is negligible. Phasematching is achieved for a 0.8 W peak power, which corresponds to an average power of only 0.13 mW. Simulation of the spectral density is given in Fig. 5 in a 10 cm long microwire section, where the walk-off length between the two pump pulses is now so large as to be effectively infinite. Both the high intrinsic $\chi^{(3)}$ of the chalcogenide and the strong confinement allows to reach a conversion efficiency of $\eta = 1.1 \times 10^{-3}$. However, as in the silica microstructured fibers, caution must be taken in filtering the desired photons, since high nonlinearity means high Raman noise, large phase modulation broadening and other undesired

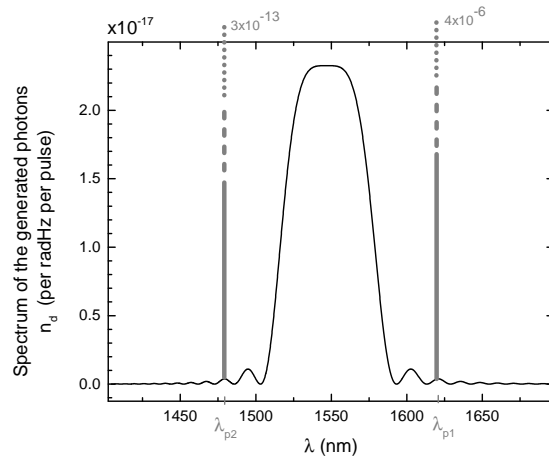


FIG. 5. Due to high intrinsic $\chi^{(3)}$ and strong confinement, the chalcogenide microwire gives the highest conversion rate, with an efficiency of $\eta = 1.1 \times 10^{-3}$. The grey lines represent the pumps' wavelengths, widths (3.1 rad THz) and intensity as in Fig. 3.

interactions such as degenerate FWM from the strong pump.

D. Experiments

Tests in our lab have shown that the nonlinear interaction in standard birefringent fibers is indeed very weak, making them unsuitable for single photon conversion. The implementation in Ref. [14] in birefringent microstructured fibers allowed an inferred conversion efficiency of 3×10^{-9} , with the weak pump kept at $4.8 \mu\text{W}$ effective average power, well above the single-photon level. This was achieved for strong pump average powers under 100 mW and employed narrowband birefringent phasematching, limiting conversion efficiency, but demonstrating the principle of single photon conversion. Finally, we have performed preliminary experiments on the chalcogenide microwires, verifying nondegenerate, external pumping phasematching conditions very similar to those shown above.

V. CONCLUSION

We have predicted a promising result in the conversion of single photons into pairs via four-wave mixing. As shown from our simulations based on evolution of the quantum field operators, conversion efficiencies up to 0.1% should be achievable in chalcogenide microwires. The results in the three types of fibers we modeled are summarized in Table I.

In this work, the low gain approximation is sufficient for applications in generating large entangled states and

Fiber type	Average pump power (mW)	Conversion efficiency η	Photon pairs per second
Biref. (silica)	5000	2×10^{-8}	1.6
Microstr. (silica)	1000	4×10^{-4}	32,000
Microwire (As ₂ Se ₃)	0.13	1×10^{-3}	80,000

TABLE I. Summary of expected single photon to pair conversion efficiency and strong pump power required for the three fiber types considered: birefringent silica fibers, microstructured silica fibers, and chalcogenide As₂Se₃ microwired fibers. Considering the 80 MHz repetition rate and inputting one photon per pulse, we also calculate the number of pairs produced per second.

photon heralding, though a non-perturbative approach keeping all orders of gain would make for an interesting study and allow exploring the deterministic pair generation $|1\rangle_{p2} \rightarrow |11\rangle_{si}$ and oscillatory $|1\rangle_{p2} \rightarrow |11\rangle_{si} \rightarrow |1\rangle_{p2} \rightarrow \dots$ regimes. However, finding a material enabling photon conversion with an efficiency high enough to justify this non-perturbative approach remains a challenge.

Interestingly, neither the derivation nor value of the conversion efficiency we found depend on the single photon being quantized: the result can equally be obtained by assuming a classical pulse with the same input peak power as the single photon. This implies there is no new quantumness in this process, beyond the well-established spontaneous generation of pairs in standard spontaneous FWM or SPDC.

In implementations, caution must be paid to the various sources of noise possible: degenerate FWM and spontaneous Raman scattering [27] from the strong pump, and even second orders or combinations of these effects.

ACKNOWLEDGMENTS

We thank Piotr Kolenderski for helpful comments and acknowledge support from NSERC (CGS, Discovery, CREATE, RTI), Ontario Ministry of Research and Innovation, CIFAR, FedDev Ontario, Industry Canada, and CFI. The authors are thankful to Coractive High-Tech for providing the chalcogenide glass used in the experiments.

Appendix A: Derivation of momentum generators

The two pumps are considered monochromatic or quasi-monochromatic, perfectly overlapping, of identical pulse duration and spectral width $\delta\omega$. The quantization time is chosen as the transform-limited pulse duration, $T = 2\pi/\delta\omega$.

The quantum field operator can be written in the continuous limit as

$$\hat{E}(z, t) = \int d\omega \sqrt{\Omega(\omega)} \hat{a}(\omega, z) e^{-i\omega t} + h.c. \quad (A1)$$

where the integral runs from zero to infinity, with the notation simplified by the introduction of the variable $\Omega(\omega) = \frac{\hbar\omega}{4\pi\epsilon_0 c A_{eff} n(\omega)}$.

The momentum operator is given by Eq. (4), from which we can derive its linear part $\hat{G}_l(z)$ and nonlinear part $\hat{G}_{nl}(z)$.

$$\begin{aligned} \hat{G}_l(z) &= \int_{A_{eff}} dS \int_0^{+T} dt \iint d\omega d\omega' \epsilon_0 \left(\chi^{(1)}(\omega) + 1 \right) \\ &\quad \times \sqrt{\Omega(\omega)} \hat{a}^\dagger(\omega, z) e^{i\omega t} \sqrt{\Omega(\omega')} \hat{a}(\omega', z) e^{-i\omega' t} + h.c. \\ &= 2A_{eff} \iint d\omega d\omega' \epsilon_0 n(\omega)^2 \Omega(\omega) \hat{a}^\dagger(\omega, z) \hat{a}(\omega, z) \\ &\quad \times 2\pi\delta(\omega - \omega') \\ &= 4\pi A_{eff} \epsilon_0 \int d\omega n(\omega)^2 \Omega(\omega) \hat{a}^\dagger(\omega, z) \hat{a}(\omega, z) \\ &= \int d\omega \frac{\hbar\omega}{c} n(\omega) \hat{a}^\dagger(\omega, z) \hat{a}(\omega, z) \end{aligned}$$

where we used $\int_0^T dt e^{i(\omega - \omega')t} = 2\pi\delta(\omega - \omega')$ (since the integration time matches the quantization time). The linear evolution of any annihilation operator can thus be deduced as in Eq. (7). The nonlinear momentum operator evolves according to

$$\hat{G}_{nl}(z) = \int_{A_{eff}} dS \int_0^{+T} dt \hat{P}_{nl}^{(-)}(z, t) \hat{E}^{(+)}(z, t) + h.c.. \quad (A2)$$

If we only consider FWM as generating propagating modes, the relevant nonlinear polarization is $\hat{P}_{nl}(z, t) = \epsilon_0 \chi^{(3)} \hat{E}^3(z, t)$. We can decompose $\hat{G}_{nl}(z)$ into two parts, one for FWM and the other for phase modulation, as $\hat{G}_{nl}(z) = \hat{G}_{nl}^{FWM}(z) + \hat{G}_{nl}^{PhMod}(z)$. Then

$$\begin{aligned} \hat{G}_{nl}(z) &= \epsilon_0 \chi^{(3)} \int_{A_{eff}} dS \int_0^{+T} dt \left[\int d\omega \sqrt{\Omega(\omega)} \hat{a}^\dagger(\omega, z) e^{i\omega t} + h.c. \right] \\ &\quad \times \left[\int d\omega' \sqrt{\Omega(\omega')} \hat{a}^\dagger(\omega', z) e^{i\omega' t} + h.c. \right] \\ &\quad \times \left[\int d\omega'' \sqrt{\Omega(\omega'')} \hat{a}^\dagger(\omega'', z) e^{i\omega'' t} + h.c. \right] \\ &\quad \times \left[\int d\omega''' \sqrt{\Omega(\omega''')} \hat{a}^\dagger(\omega''', z) e^{i\omega''' t} + h.c. \right]. \quad (A3) \end{aligned}$$

We keep only the frequencies that will propagate in the fiber: the frequencies around the two pumps, and frequencies generated by FWM with these 2 pumps. We can separate the operators into four frequency parts

$$\begin{aligned}
& \int d\omega \sqrt{\Omega(\omega)} \hat{a}(\omega, z) e^{-i\omega t} = \\
& \int_{\Delta\omega_{p1}} d\omega_1 \sqrt{\Omega(\omega_1)} \hat{a}(\omega_1, z) e^{-i\omega_1 t} \\
& + \int_{\Delta\omega_{p2}} d\omega_2 \sqrt{\Omega(\omega_2)} \hat{a}(\omega_2, z) e^{-i\omega_2 t} \\
& + \int_{\Delta\omega_s} d\omega \sqrt{\Omega(\omega)} \hat{a}(\omega, z) e^{-i\omega t} \\
& + \int_{\Delta\omega_i} d\omega' \sqrt{\Omega(\omega')} \hat{a}(\omega', z) e^{-i\omega' t},
\end{aligned} \tag{A4}$$

where $\Delta\omega_s$ and $\Delta\omega_i$ are a wide frequency range around the central frequencies of the photon pairs generated by FWM and $\Delta\omega_{p1,p2}$ are a wide range frequency around the two pump wavelengths. Since we assumed our two pumps are monochromatic or quasi-monochromatic and took their bandwidth as the frequency step $\Delta\omega_{p1} = \Delta\omega_{p2} = \delta\omega = 2\pi/T$, we can write $\int_{\Delta\omega_{p1}} d\omega_1 \sqrt{\Omega(\omega_1)} \hat{a}(\omega_1, z) =$

$\delta\omega \sqrt{\Omega(\omega_{p1})} \hat{a}(\omega_{p1}, z) = \frac{2\pi}{T} \sqrt{\Omega(\omega_{p1})} \hat{a}(\omega_{p1}, z)$ with ω_{p1} the central frequency of pump 1, and the same for pump 2. For more clarity in the expressions with respect to the other operators, we keep the pump mode operators dimensioned as $[\hat{a}(\omega_{p1,p2}, z)] = \sqrt{\frac{1}{\delta\omega}}$, so the number of pump photons travelling through a plane of position z during the time interval T is $\frac{2\pi}{T} \langle \hat{a}^\dagger(\omega_{p1,2}, z) \hat{a}(\omega_{p1,2}, z) \rangle$. Then we can write

$$\begin{aligned}
& \int d\omega \sqrt{\Omega(\omega)} \hat{a}(\omega, z) e^{-i\omega t} = \\
& \frac{2\pi}{T} \left[\sqrt{\Omega(\omega_{p1})} \hat{a}(\omega_{p1}, z) e^{-i\omega_{p1} t} + \sqrt{\Omega(\omega_{p2})} \hat{a}(\omega_{p2}, z) e^{-i\omega_{p2} t} \right] \\
& + \int_{\Delta\omega_s} d\omega \sqrt{\Omega(\omega)} \hat{a}(\omega, z) e^{-i\omega t} \\
& + \int_{\Delta\omega_i} d\omega' \sqrt{\Omega(\omega')} \hat{a}(\omega', z) e^{-i\omega' t}.
\end{aligned} \tag{A5}$$

The FWM part of the nonlinear momentum is then

$$\begin{aligned}
\hat{G}_{nl}^{FWM}(z) &= 24 \times \left(\frac{2\pi}{T} \right)^2 \varepsilon_0 \chi^{(3)} \int_{A_{eff}} dS \int_0^{+T} dt \int_{\Delta\omega_s} d\omega \sqrt{\Omega(\omega)} \hat{a}^\dagger(\omega, z) \\
&\times \int_{\Delta\omega_i} d\omega' \sqrt{\Omega(\omega')} \hat{a}^\dagger(\omega', z) \sqrt{\Omega(\omega_{p1})} \hat{a}(\omega_{p1}, z) \sqrt{\Omega(\omega_{p2})} \hat{a}(\omega_{p2}, z) e^{i\Delta\omega t} + h.c.
\end{aligned}$$

or, if we write the operators as product of their linear and nonlinear parts,

$$\begin{aligned}
\hat{G}_{nl}^{FWM}(z) &= 24 \times \left(\frac{2\pi}{T} \right)^2 \varepsilon_0 \chi^{(3)} \int_{A_{eff}} dS \int_0^{+T} dt \int_{\Delta\omega_s} d\omega \sqrt{\Omega(\omega)} \hat{a}_0^\dagger(\omega, z) \\
&\times \int_{\Delta\omega_i} d\omega' \sqrt{\Omega(\omega')} \hat{a}_0^\dagger(\omega', z) \sqrt{\Omega(\omega_{p1})} \hat{a}_0(\omega_{p1}, z) \sqrt{\Omega(\omega_{p2})} \hat{a}_0(\omega_{p2}, z) e^{i\Delta\omega t} e^{-i\Delta k z} + h.c..
\end{aligned}$$

The factor 24 comes from all the possible combinations of the mode operators. Here $\Delta\omega = \omega + \omega' - \omega_{p1} - \omega_{p2}$ and $\Delta k = \beta(\omega) + \beta(\omega') - \beta(\omega_{p1}) - \beta(\omega_{p2})$. Using again $\int_0^T dt e^{i\Delta\omega t} = 2\pi\delta(\Delta\omega)$ and $\int d\omega' \delta(\Delta\omega) = 1$, and evaluating the cross-sectional area integral, we have

$$\begin{aligned}
\hat{G}_{nl}^{FWM}(z) &= 24 \times 2\pi \times \left(\frac{2\pi}{T} \right)^2 \varepsilon_0 \chi^{(3)} A_{eff} \sqrt{\Omega(\omega_{p1})} \sqrt{\Omega(\omega_{p2})} \int_{\Delta\omega_s} d\omega \sqrt{\Omega(\omega)} \sqrt{\Omega(\omega_{p1} + \omega_{p2} - \omega)} \times \\
&\hat{a}_0^\dagger(\omega, z) \hat{a}_0^\dagger(\omega_{p1} + \omega_{p2} - \omega, z) \times \hat{a}_0(\omega_{p1}, z) \hat{a}_0(\omega_{p2}, z) e^{-i\Delta k z} + h.c..
\end{aligned} \tag{A6}$$

We can extend the integral over the signal over the whole spectrum except the two pumps' frequencies and add a factor 1/2 for double-counting signal and idler frequencies. Then

$$\begin{aligned}
\hat{G}_{nl}^{FWM}(z) &= 3 \times \frac{2\pi}{T} \chi^{(3)} \frac{\hbar^2}{\varepsilon_0 c^2 A_{eff} T} \sqrt{\frac{\omega_{p1}}{n(\omega_{p1})} \frac{\omega_{p2}}{n(\omega_{p2})}} \\
&\times \int d\omega \sqrt{\frac{\omega}{n(\omega)}} \sqrt{\frac{\omega_{p1} + \omega_{p2} - \omega}{n(\omega_{p1} + \omega_{p2} - \omega)}} \hat{a}_0^\dagger(\omega, z)
\end{aligned} \tag{A7}$$

$$\times \hat{a}_0^\dagger(\omega_{p1} + \omega_{p2} - \omega, z) \hat{a}_0(\omega_{p1}, z) \hat{a}_0(\omega_{p2}, z) e^{-i\Delta k z} + h.c..$$

Now let's look for the phase modulation term. By definition of phase modulation, we keep only the terms with no phase that arise from the expansion (A3) of the nonlinear momentum. We then obtain :

$$\hat{G}_{nl}^{ph\ mod}(z) = \int_{A_{eff}} dS \varepsilon_0 \chi^{(3)} \times \tag{A8}$$

$$\begin{aligned}
& \left[6 \times \left(\frac{2\pi}{T} \right) \sum_{k=s,i,p_1,p_2} \left(\int_{\Delta\omega_k} d\omega \Omega(\omega) \hat{a}_0^\dagger(\omega, z) \hat{a}_0(\omega, z) \right)^2 + \right. \\
& 12 \times \left(\frac{2\pi}{T} \right) \sum_{k=s,i,p_1,p_2} \sum_{j \neq k} \left(\frac{2\pi}{T} \right) \int_{\Delta\omega_k} d\omega \int_{\Delta\omega_j} d\omega' \\
& \left. \Omega(\omega) \Omega(\omega') \hat{a}_0^\dagger(\omega, z) \hat{a}_0(\omega', z) \hat{a}_0^\dagger(\omega', z) \hat{a}_0(\omega, z) \right],
\end{aligned}$$

or

$$\hat{G}_{nl}^{ph\ mod}(z) = 3\chi^{(3)} \frac{\hbar^2}{\varepsilon_0 c^2 A_{eff} T} \left[\iint d\omega d\omega' \frac{\omega}{n(\omega)} \frac{\omega'}{n(\omega')} \hat{a}_0^\dagger(\omega, z) \hat{a}_0(\omega', z) \hat{a}_0^\dagger(\omega', z) \hat{a}_0(\omega, z) - \frac{1}{2} \int d\omega \frac{2\pi}{T} \left(\frac{\omega}{n(\omega)} \hat{a}_0^\dagger(\omega, z) \hat{a}_0(\omega, z) \right)^2 \right]. \quad (A10)$$

and if we sum over all the frequencies in the integrals, the momentum generator collapses into

$$\hat{G}_{nl}^{ph\ mod}(z) = \left(\frac{2\pi}{T} \right) \times 2\pi \times A_{eff} \varepsilon_0 \chi^{(3)} \times \left[12 \iint d\omega d\omega' \Omega(\omega) \Omega(\omega') \hat{a}_0^\dagger(\omega, z) \hat{a}_0(\omega', z) \hat{a}_0^\dagger(\omega', z) \hat{a}_0(\omega, z) - 6 \int d\omega \frac{2\pi}{T} \left(\Omega(\omega) \hat{a}_0^\dagger(\omega, z) \hat{a}_0(\omega, z) \right)^2 \right] \quad (A9)$$

Appendix B: Low gain approximation and derivation of mode operators

We can now derive the mode operators from Eq. (3), for any frequency generated in the fiber, which gives Eqs. (10), (11), and (12).

We proceed by first factoring out the phase modulation with the variable change $\hat{a}_0(\omega, z) = \hat{a}'_0(\omega, z) e^{i2\gamma P_1 z}$, which gives for the generated modes' FWM evolution

$$\begin{aligned}
& \frac{\partial \hat{a}'_0(\omega, z)}{\partial z} e^{i2\gamma P_1 z} + i2\gamma P_1 \hat{a}'_0(\omega, z) e^{i2\gamma P_1 z} = \\
& 2i\gamma \times \sqrt{P_1} \sqrt{\zeta_2} \times \hat{a}'_0^\dagger(\omega_{p1} + \omega_{p2} - \omega, z) \hat{a}'_0(\omega_{p2}, z) e^{-i(\Delta k - \gamma P_1)z} + 2i\gamma \times P_1 \hat{a}'_0(\omega, z) e^{i2\gamma P_1 z}
\end{aligned} \quad (B1)$$

so

$$\frac{\partial \hat{a}'_0(\omega, z)}{\partial z} = 2i\gamma \times \sqrt{P_1} \sqrt{\zeta_2} \times \hat{a}'_0^\dagger(\omega_{p1} + \omega_{p2} - \omega, z) \hat{a}'_0(\omega_{p2}, z) e^{-i(\Delta k + \gamma P_1)z}. \quad (B2)$$

For the weak pump it gives

$$\frac{\partial \hat{a}'_0(\omega_{p2}, z)}{\partial z} e^{i2\gamma P_1 z} + i2\gamma P_1 \hat{a}'_0(\omega_{p2}, z) e^{i2\gamma P_1 z} = \quad (B3)$$

$$2i\gamma \times P_1 \hat{a}'_0(\omega_{p2}, z) e^{i2\gamma P_1 z} + 2i\gamma \times \sqrt{P_1} \sqrt{\zeta_2} \times \frac{T}{2\pi} \times \int d\omega \sqrt{\frac{\omega(\omega_{p1} + \omega_{p2} - \omega)}{\omega_{p1}\omega_{p2}}} \hat{a}'_0(\omega, z) \hat{a}'_0(\omega_{p1} + \omega_{p2} - \omega, z) e^{i(\Delta k + \gamma P_1)z},$$

or

$$\frac{\partial \hat{a}'_0(\omega_{p2}, z)}{\partial z} = 2i\gamma \times \sqrt{P_1} \sqrt{\zeta_2} \times \frac{T}{2\pi} \int d\omega \sqrt{\frac{\omega(\omega_{p1} + \omega_{p2} - \omega)}{\omega_{p1}\omega_{p2}}} \hat{a}'_0(\omega, z) \hat{a}'_0(\omega_{p1} + \omega_{p2} - \omega, z) e^{i(\Delta k + \gamma P_1)z}. \quad (B4)$$

The total phase mismatch is now $K = \Delta k + \gamma P_1$. The modes' evolution can be solved by performing a Baker-Hausdorff expansion. If the z evolution of the momentum operator $\hat{G}(z)$ is slow enough to be considered as z independent, which is the case in a low gain interaction, $\int_0^L \hat{G}_{nl}(z) dz \simeq \hat{G}_{nl} L$ and $\hat{a}_0(\omega, L) = e^{-\frac{i}{\hbar} \hat{G}_{nl} L} \hat{a}_0(\omega, 0) e^{+\frac{i}{\hbar} \hat{G}_{nl} L}$, which gives

$$\begin{aligned}
\hat{a}_0(\omega, L) &= \hat{a}_0(\omega, 0) + \left[\hat{a}_0(\omega, 0), \frac{i}{\hbar} \hat{G}_{nl} L \right] + \\
& \frac{1}{2!} \left[\left[\hat{a}_0(\omega, 0), \frac{i}{\hbar} \hat{G}_{nl} L \right], \frac{i}{\hbar} \hat{G}_{nl} L \right] + \quad (B5)
\end{aligned}$$

$$\frac{1}{3!} \left[\left[\left[\hat{a}_0(\omega, 0), \frac{i}{\hbar} \hat{G}_{nl} L \right], \frac{i}{\hbar} \hat{G}_{nl} L \right], \frac{i}{\hbar} \hat{G}_{nl} L \right] + \dots$$

or, given that $\frac{i}{\hbar} \left[\hat{a}_0(\omega, 0), \hat{G}_{nl}(L) \right] = \left(\frac{\partial \hat{a}_0(\omega, z)}{\partial z} \right)_{z=0}$,

$$\begin{aligned}
\hat{a}_0(\omega, L) &= \hat{a}_0(\omega, 0) + \left(\frac{\partial \hat{a}_0(\omega, z)}{\partial z} \right)_{z=0} L + \\
& \left(\frac{\partial^2 \hat{a}_0(\omega, z)}{\partial z^2} \right)_{z=0} \frac{L^2}{2!} + \left(\frac{\partial^3 \hat{a}_0(\omega, z)}{\partial z^3} \right)_{z=0} \frac{L^3}{3!} + \dots \quad (B6)
\end{aligned}$$

This development (B6), equivalent to a Taylor expansion for the operators, gives the creation and annihilation operators at the output of the medium for the generated

modes and the weak pump, solutions of Eqs. (B2) and (B4) respectively. Let's solve it for the generated modes.

Eq. (B2) gives for the higher order derivatives

$$\frac{\partial^2 \hat{a}'_0(\omega, z)}{\partial z^2} = \quad (B7)$$

$$\begin{aligned} & -iK \times 2i\gamma\sqrt{P_1}\sqrt{\zeta_2}\hat{a}_0'^{\dagger}(\omega_{p1} + \omega_{p2} - \omega, z)\hat{a}'_0(\omega_{p2}, z)e^{-iKz} + \\ & 2i\gamma\sqrt{P_1}\sqrt{\zeta_2} \times \frac{\partial \hat{a}_0'^{\dagger}(\omega_{p1} + \omega_{p2} - \omega, z)}{\partial z}\hat{a}'_0(\omega_{p2}, z)e^{-iKz} + \\ & 2i\gamma\sqrt{P_1}\sqrt{\zeta_2} \times \hat{a}_0'^{\dagger}(\omega_{p1} + \omega_{p2} - \omega, z)\frac{\partial \hat{a}'_0(\omega_{p2}, z)}{\partial z}e^{-iKz} \end{aligned}$$

so

$$\begin{aligned} \frac{\partial^2 \hat{a}'_0(\omega, z)}{\partial z^2} = \quad (B8) \\ -iK \times 2i\gamma\sqrt{P_1}\sqrt{\zeta_2}\hat{a}_0'^{\dagger}(\omega_{p1} + \omega_{p2} - \omega, z)\hat{a}'_0(\omega_{p2}, z)e^{-iKz} + \\ \left(2i\gamma\sqrt{P_1}\sqrt{\zeta_2}\right)^2 \times \hat{a}_0'^{\dagger}(\omega, z)\hat{a}'_0(\omega_{p2}, z)\hat{a}'_0(\omega_{p2}, z)e^{-iKz}e^{iKz} + \end{aligned}$$

$$\left(2i\gamma\sqrt{P_1}\sqrt{\zeta_2}\right)^2 \times \frac{T}{2\pi} \int d\omega \sqrt{\frac{\omega(\omega_{p1} + \omega_{p2} - \omega)}{\omega_{p1}\omega_{p2}}} \times \hat{a}_0'^{\dagger}(\omega_{p1} + \omega_{p2} - \omega, z)\hat{a}'_0(\omega, z)\hat{a}'_0(\omega_{p1} + \omega_{p2} - \omega, z)e^{-iKz}e^{-iKz}.$$

The quantity $\gamma \times \sqrt{P_1}\sqrt{\frac{T}{2\pi}\zeta_2}$ being very small (it is the square root number of photons generated in 1 meter of medium within a frequency range of $\delta\omega$, see the link to the efficiency η in Eq. (28)), we will limit our development to the first order in $\gamma \times \sqrt{P_1}\sqrt{\frac{T}{2\pi}\zeta_2}$. This approximation is physically equivalent to neglecting all the phenomena involving more than a single pair creation, in particular here the recombination of a created pair back into pump photons, and the Rabi oscillations that can then occur between signal/idler and pump photon states. Then we have

$$\frac{\partial^2 \hat{a}'_0(\omega, z)}{\partial z^2} = -iK \times 2i\gamma\sqrt{P_1}\sqrt{\zeta_2} \times \hat{a}_0'^{\dagger}(\omega_{p1} + \omega_{p2} - \omega, z)\hat{a}'_0(\omega_{p2}, z)e^{-iKz}. \quad (B9)$$

By doing the same approximation for the third order we get

$$\frac{\partial^3 \hat{a}'_0(\omega, z)}{\partial z^3} = (-iK)^2 2i\gamma\sqrt{P_1}\sqrt{\zeta_2} \times \hat{a}_0'^{\dagger}(\omega_{p1} + \omega_{p2} - \omega, z)\hat{a}'_0(\omega_{p2}, z)e^{-iKz}, \quad (B10)$$

and by an obvious recurrence

$$\frac{\partial^n \hat{a}'_0(\omega, z)}{\partial z^n} = (-iK)^{n-1} 2i\gamma\sqrt{P_1}\sqrt{\zeta_2} \times \hat{a}_0'^{\dagger}(\omega_{p1} + \omega_{p2} - \omega, z)\hat{a}'_0(\omega_{p2}, z)e^{-iKz}. \quad (B11)$$

Then Eq. (B6) gives

$$\hat{a}'_0(\omega, L) = \hat{a}'_0(\omega, 0) + 2i\gamma\sqrt{P_1}\sqrt{\zeta_2}\hat{a}_0'^{\dagger}(\omega_{p1} + \omega_{p2} - \omega, 0)\hat{a}'_0(\omega_{p2}, 0)e^{-iKL} \sum_{n=1}^{+\infty} \frac{L^n}{n!} (-iK)^{n-1}.$$

The power series can be simplified to

$$\sum_{n=1}^{+\infty} \frac{L^n}{n!} (-iK)^{n-1} = L \sum_{n=1}^{+\infty} \frac{(-iKL)^{n-1}}{n!} = L \frac{e^{-iKL} - 1}{-iKL} = e^{-\frac{iKL}{2}} L \text{sinc}\left(\frac{KL}{2}\right), \quad (B12)$$

so

$$\hat{a}'_0(\omega, L) = \hat{a}'_0(\omega, 0) + 2i\gamma \times \sqrt{P_1}\sqrt{\zeta_2}e^{-\frac{iKL}{2}} L \times \text{sinc}\left(\frac{KL}{2}\right) \times \hat{a}_0'^{\dagger}(\omega_{p1} + \omega_{p2} - \omega, 0)\hat{a}'_0(\omega_{p2}, 0).$$

Then with $\hat{a}_0(\omega, z) = \hat{a}'_0(\omega, z)e^{i2\gamma P_1 z}$,

$$\hat{a}_0(\omega, L)e^{-i2\gamma P_1 L} = \hat{a}_0(\omega, 0) + 2i\gamma\sqrt{P_1}\sqrt{\zeta_2}e^{-\frac{iKL}{2}} L \times \text{sinc}\left(\frac{KL}{2}\right) \hat{a}_0^{\dagger}(\omega_{p1} + \omega_{p2} - \omega, 0)\hat{a}_0(\omega_{p2}, 0).$$

Appendix C: Validity of low gain approximation

In Appendix B we developed the creation and annihilation operator evolution to the first order in the gain.

If η , as defined in Eq. (28), is much less than 1, it is the efficiency of conversion of a single photon into a pair. Searching for the precision of this result, we have to go to higher orders in gain in the development of Appendix B.

Going to the second order in η allows the possibility of having a pair converted back into a single photon, which occurs with probability η^2 , but the forward single photon conversion efficiency is unchanged. Going to the third order in η then lowers the single photon conversion efficiency to $\eta - 2\eta^2 + \eta^3$. This result allows us to define the error due to taking the gain to first order as $2\eta^2$.

In principle, η could have an arbitrarily large value by increasing the strong pump power. When η approaches and goes beyond 1, it cannot be defined as a probability of

conversion, and we must solve exactly the operator evolution. As developed in a classical setting in Ref. [28], elliptic functions are expected for the beams' intensity evolution, giving Rabi-like oscillations between the pump photon and the signal/idler pair state. As noted in Ref. [14], the higher the η , the more oscillations will occur in the fiber, but this is again a theoretical scheme taking only nondegenerate FWM into account. Parasitic phenomena, in particular self-phase modulation, will also become ultra high in this regime.

-
- [1] D. C. Burnham and D. L. Weinberg, Phys. Rev. Lett. **25**, 84 (1970).
 - [2] M. Fiorentino, P. Voss, J. Sharping, and P. Kumar, IEEE Photonics Technology Letters **14**, 983 (2002).
 - [3] T. Guerreiro, E. Pomarico, B. Sanguinetti, N. Sangouard, J. S. Pelc, C. Langrock, M. M. Fejer, H. Zbinden, R. T. Thew, and N. Gisin, Nat. Commun. **4**, 2324 (2013).
 - [4] D. R. Hamel, L. K. Shalm, H. Hübel, A. J. Miller, F. Marsili, V. B. Verma, R. P. Mirin, S. W. Nam, K. J. Resch, and T. Jennewein, ArXiv e-prints (2014), arXiv:1404.7131 [quant-ph].
 - [5] Y. Miwa, J.-i. Yoshikawa, N. Iwata, M. Endo, P. Marek, R. Filip, P. van Loock, and A. Furusawa, Phys. Rev. Lett. **113**, 013601 (2014).
 - [6] H. Huebel, D. R. Hamel, A. Fedrizzi, S. Ramelow, K. J. Resch, and T. Jennewein, Nature **466**, 601 (2010).
 - [7] L. K. Shalm, D. R. Hamel, Z. Yan, C. Simon, K. J. Resch, and T. Jennewein, Nat. Phys. **9**, 19 (2013).
 - [8] D. E. Browne and T. Rudolph, Phys. Rev. Lett. **95**, 010501 (2005).
 - [9] M. Hillery, V. Buzek, and A. Berthiaume, Phys. Rev. A **59**, 1829 (1999).
 - [10] K. Banaszek and P. L. Knight, Phys. Rev. A **55**, 2368 (1997).
 - [11] D. M. Greenberger, M. A. Horne, A. Shimony, and A. Zeilinger, Am. J. Phys. **58**, 1131 (1990).
 - [12] A. Cabello and F. Sciarrino, Phys. Rev. X **2**, 21010 (2012).
 - [13] N. Gisin, S. Pironio, and N. Sangouard, Phys. Rev. Lett. **105**, 070501 (2010).
 - [14] N. K. Langford, S. Ramelow, R. Prevedel, W. J. Munro, G. J. Milburn, and A. Zeilinger, Nature **478**, 360 (2011).
 - [15] S. Tanzilli, H. De Riedmatten, W. Tittel, H. Zbinden, P. Baldi, M. De Micheli, D. B. Ostrowsky, and N. Gisin, Electron. Lett. **37**, 26 (2001).
 - [16] E. Brainin, Physical Review A **79**, 023840 (2009).
 - [17] Q. Lin, F. Yaman, and G.P. Agrawal, Physical Review A **75**, 023803 (2007).
 - [18] B. Huttner, S. Serulnik, and Y. Ben-Aryeh, Phys. Rev. A **42**, 5594 (1990).
 - [19] K. J. Blow, R. Loudon, S. J. D. Phoenix, and T. J. Shepherd, Phys. Rev. A **42**, 4102 (1990).
 - [20] G. Agrawal, *Nonlinear Fiber Optics*, 4th ed. (Academic Press, 2006).
 - [21] Material absorption can be included here and in all the following evolutions by taking z as the effective position in the fiber; $z = \frac{1-e^{-\alpha z'}}{\alpha}$ for absorption coefficient α and true position z' .
 - [22] B. J. Smith, P. Mahou, O. Cohen, J. S. Lundeen, and I. A. Walmsley, Opt. Express **17**, 23589 (2009).
 - [23] J. Rarity, J. Fulconis, J. Duligall, W. Wadsworth, and P. Russell, Opt. Express **13**, 534 (2005).
 - [24] C. Baker and M. Rochette, IEEE Photonics Journal **4**, 960 (2012).
 - [25] R. Ahmad and M. Rochette, Opt. Express **20**, 9572 (2012).
 - [26] G. Lenz, J. Zimmermann, T. Katsufuji, M. E. Lines, H. Y. Hwang, S. Spälter, R. E. Slusher, S.-W. Cheong, J. Sanghera, and I. D. Aggarwal, Opt. Letters **25**, 254 (2000).
 - [27] A. S. Clark, M. J. Collins, A. C. Judge, E. C. Mägi, C. Xiong, and B. J. Eggleton, Opt. Express **20**, 16807 (2012).
 - [28] Y. Chen, Journal of the Optical Society of America B **6**, 1986 (1989).